THE JOURNAL OF BIOLOGICAL CHEMISTRY VOL. 291, NO. 39, pp. 20427–20439, September 23, 2016

Retinal Hypercholesterolemia Triggers Cholesterol Accumulation and Esterification in Photoreceptor Cells*

Received for publication, June 21, 2016, and in revised form, August 5, 2016 Published, JBC Papers in Press, August 11, 2016, DOI 10.1074/jbc.M116.744656

Aicha Saadane[‡], Natalia Mast[‡], Tung Dao[‡], Baseer Ahmad[‡§], and Irina A. Pikuleva[‡1]

From the [‡]Department of Ophthalmology and Visual Sciences, Case Western Reserve University, Cleveland, Ohio and the [§]University Hospitals, Cleveland, Ohio 44106

The process of vision is impossible without the photoreceptor cells, which have a unique structure and specific maintenance of cholesterol. Herein we report on the previously unrecognized cholesterol-related pathway in the retina discovered during follow-up characterizations of *Cyp27a1*$^{-/-}$*Cyp46a1*$^{-/-}$ mice. These animals have retinal hypercholesterolemia and convert excess retinal cholesterol into cholesterol esters, normally present in the retina in very small amounts. We established that in the *Cyp27a1*$^{-/-}$*Cyp46a1*$^{-/-}$ retina, cholesterol esters are generated by and accumulate in the photoreceptor outer segments (OS), which is the retinal layer with the lowest cholesterol content. Mouse OS were also found to express the cholesterol-esterifying enzyme acyl-coenzyme A:cholesterol acyltransferase (ACAT1), but not lecithin-cholesterol acyltransferase (LCAT), and to differ from humans in retinal expression of ACAT1. Nevertheless, cholesterol esters were discovered to be abundant in human OS. We suggest a mechanism for cholesterol ester accumulation in the OS and that activity impairment of ACAT1 in humans may underlie the development of subretinal drusenoid deposits, a hallmark of age-related macular degeneration, which is a common blinding disease. We generated *Cyp27a1*$^{-/-}$*Cyp46a1*$^{-/-}$*Acat1*$^{-/-}$ mice, characterized their retina by different imaging modalities, and confirmed that unesterified cholesterol does accumulate in their OS and that there is photoreceptor apoptosis and OS degeneration in this line. Our results provide insights into the retinal response to local hypercholesterolemia and the retinal significance of cholesterol esterification, which could be cell-specific and both beneficial and detrimental for retinal structure and function.

Photoreceptor (PR)[2] cells, rods and cones, are highly specialized neurons that initiate the transmission of the visual signal to the brain. These cells are localized exclusively to the retina, a multilayered structure lining the inner surface of the eye. Vertebrate PR cells have a unique polarized morphology that includes the outer segment (OS), formed by stacks of discs responsible for light capture and the transmission of visual signal; the inner segment (IS), rich in mitochondria to provide the cell with energy; the nucleus-containing soma; the axon; and the synaptic terminal (1). Because PR cells are essential for light perception, their dysfunction affects vision, and their loss due to degeneration causes irreversible blindness (2).

Not only do the PR cells have a unique structure, but they also have very specific maintenance of cholesterol as indicated by the lack of the key proteins of cholesterol biosynthesis, uptake, metabolism, efflux, and regulation (3, 4). Cholesterol distribution within PR cells is also unique; it is uneven (3, 5) and forms a gradient with a higher sterol concentration at the IS/OS border and a lower cholesterol concentration at the tip of the OS embraced by apical processes of the retinal pigment epithelium (RPE) (6). The reason for such unique maintenance and distribution of cholesterol in the PR cells is currently unknown but could be due to the inhibitory effect of cholesterol on the efficiency of the phototransduction cascade initiated in the OS (7, 8). OS phagocytosis by the RPE could be a factor as well, because it accounts for ~10% of daily OS renewal (9). Accordingly, the tip of the OS has adapted to contain low cholesterol content to minimize daily retinal cholesterol loss from phagocytosis and the amount of cholesterol that has to be replenished (3).

Cholesterol maintenance in the retina has been linked to age-related macular degeneration (AMD) (5), a devastating blinding disease in the elderly of the industrialized world (10). Drusen and subretinal drusenoid deposits (SDD), the two major hallmarks of AMD, contain large amounts of cholesterol (11–13) and develop below the RPE (14) and at the OS/RPE interface, respectively (15). Accordingly, the OS may be involved in the biogenesis of SDD (15–17). In SDD, cholesterol is mostly unesterified (13), whereas drusen contain both unesterified cholesterol (UC) and esterified cholesterol (EC) (11, 12). Retinal sensitivity in eyes with SDD is reduced much more than in eyes with typical drusen (18, 19), and SDD accumulation has been found to be a risk factor for AMD advancement and disease severity (20–24). SDD are also associated with a higher

* This work was supported in part by National Institutes of Health Grant EY018383 (to I. A. P.), the P30 Core Grant EY11373, and by the Ohio Lions Eye Research Foundation. The authors declare that they have no conflicts of interest with the contents of this article. The content is solely the responsibility of the authors and does not necessarily represent the official views of the National Institutes of Health.

[1] Recipient of the Jules and Doris Stein Professorship from the Research to Prevent Blindness Foundation. To whom correspondence should be addressed: Dept. of Ophthalmology and Visual Sciences, Case Western Reserve University, 2085 Adelbert Rd., Rm. 303a, Cleveland, OH 44106. Tel.: 216-368-3823; Fax: 216-360-3482; E-mail: iap8@case.edu.

[2] The abbreviations used are: PR, photoreceptor; ACAT, acyl-coenzyme A: cholesterol acyltransferase; AMD, age-related macular degeneration; EC, esterified cholesterol; GCL, ganglion cell layer; GC-MS, gas chromatography-mass spectrometry; GS, glutamine synthase; IS, inner segments; LCAT, lecithin-cholesterol acyltransferase; LCM, laser capture microdissection; OPL, outer plexiform layer; OS, outer segment; RPE, retinal pigment epithelium; SDD, subretinal drusenoid deposits; SD-OCT, spectral domain optical coherence tomography; TC, total cholesterol; TEM, transmission electron microscopy; UC, unesterified cholesterol; qRT-PCR, quantitative RT-PCR.

mortality rate (25), which might be a manifestation of some systemic, perhaps inflammatory or vascular, diseases (26).

As part of our investigation of retinal cholesterol homeostasis, we generated *Cyp27a1*$^{-/-}$*Cyp46a1*$^{-/-}$ mice (27) lacking cytochromes P450 CYP27A1 and CYP46A1, responsible for the majority of cholesterol metabolism in the retina (28–31). These animals have a 1.8- and 2-fold increase in total retinal cholesterol in females and males, respectively, with more than half of this total cholesterol (TC) being esterified. This is very unusual for the neural retina, in which cholesterol is mostly (~85%) unesterified under normal conditions (29, 32). Significant cholesterol esterification in the *Cyp27a1*$^{-/-}$*Cyp46a1*$^{-/-}$ retina provided the impetus for the present work, in which we investigated retinal localization and the origin of EC in *Cyp27a1*$^{-/-}$*Cyp46a1*$^{-/-}$ mice. We found that EC is localized mainly in the *Cyp27a1*$^{-/-}$*Cyp46a1*$^{-/-}$ OS, thereby revealing a previously unrecognized, photoreceptor-specific mechanism for handling retinal cholesterol excess. Subsequent investigation of human retinas suggested that the data obtained may be of clinical relevance because they provide novel insight into the biogenesis of SDD, which is only now beginning to be investigated (13, 33).

Results

Localization of EC in Mouse Retina—Normally, EC accounts for only 14% of TC in the retina of female and male mice (Fig. 1*A*). Yet, in the retina of *Cyp27a1*$^{-/-}$*Cyp46a1*$^{-/-}$ mice, in which TC is increased from 1.8- to 2-fold depending on the gender (Fig. 1*A*), EC represents from 55% (females) to 76% (males) of TC as established by our previous measurements by gas chromatography-mass spectrometry (GC-MS) (27). To localize EC in the *Cyp27a1*$^{-/-}$*Cyp46a1*$^{-/-}$ retina, we used the fluorescent antibiotic filipin, which interacts with the 3β-hydroxyl in EC released by tissue pretreatment with cholesterol esterase (34, 35). As compared with the *Cyp27a1*$^{+/+}$*Cyp46a1*$^{+/+}$ retina, which showed no fluorescent signal for EC (Fig. 2, *A*–*C*), the *Cyp27a1*$^{-/-}$*Cyp46a1*$^{-/-}$ retina had a strong fluorescent signal for EC in the OS and much weaker fluorescent signals in the ganglion cell layer (GCL) and outer plexiform layer (OPL) (Fig. 2, *D*–*F*).

We next isolated the PR layer, containing both OS and IS, from retinal cross-sections of *Cyp27a1*$^{+/+}$*Cyp46a1*$^{+/+}$ and *Cyp27a1*$^{-/-}$*Cyp46a1*$^{-/-}$ mice by laser capture microdissection (LCM) and analyzed this layer for cholesterol content by GC-MS. TC was increased ~3-fold in the *Cyp27a1*$^{-/-}$*Cyp46a1*$^{-/-}$ PR cells relative to the *Cyp27a1*$^{+/+}$*Cyp46a1*$^{+/+}$ PR cells (Fig. 3*A*), a higher TC increase than in the whole retina (1.8–2-fold, Fig. 1*A*) suggesting that PR cells are a site for cholesterol accumulation in the *Cyp27a1*$^{-/-}$*Cyp46a1*$^{-/-}$ retina. Furthermore, an increase in TC in the *Cyp27a1*$^{-/-}$*Cyp46a1*$^{-/-}$ PR cells was because of an increase in EC, which accounted for 79% of TC in this genotype. For comparison, EC represented only 22% of TC in the *Cyp27a1*$^{+/+}$*Cyp46a1*$^{+/+}$ PR cells. Thus, sterol quantifications in mouse PR cells confirmed EC detection by histochemistry (Fig. 2*F*).

We then used transmission electron microscopy (TEM) following tannic acid and *para*-phenylenediamine treatment of the osmicated retina (11, 36). Tannic acid preserves the lipids

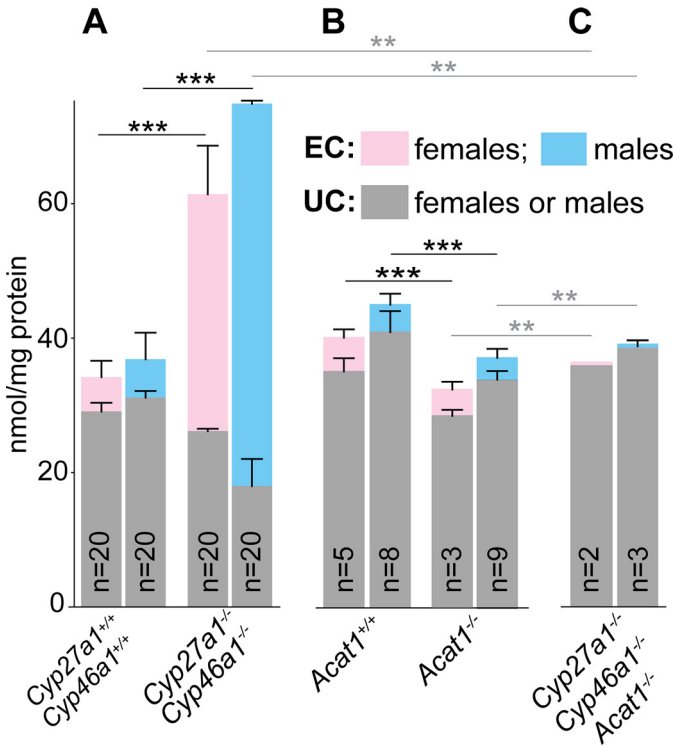

FIGURE 1. **Retinal content of EC and UC in different mouse genotypes.** *A*, the *Cyp27a1*$^{+/+}$*Cyp46a1*$^{+/+}$ and *Cyp27a1*$^{-/-}$*Cyp46a1*$^{-/-}$ lines; *B*, the *Acat1*$^{+/+}$ and *Acat1*$^{-/-}$ lines; and *C*, the *Cyp27a1*$^{-/-}$*Cyp46a1*$^{-/-}$*Acat1*$^{-/-}$ line. In all genotypes, except *Cyp27a1*$^{-/-}$*Cyp46a1*$^{-/-}$*Acat1*$^{-/-}$ females, the results are the mean ± S.D. with "*n*" being the number of animals. In *Cyp27a1*$^{-/-}$*Cyp46a1*$^{-/-}$ *Acat1*$^{-/-}$ females, the results are the mean of duplicate measurements: 35 and 36 nmol/mg protein for UC; 0.6 and 0.5 nmol/mg protein for EC. Pooled retinal samples from 4–7-month-old mice (two retinas from each) were used for triplicate measurements in the *Cyp27a1*$^{+/+}$*Cyp46a1*$^{+/+}$ and *Cyp27a1*$^{-/-}$*Cyp46a1*$^{-/-}$ genotypes. Individual retinas, one retina from each 3–5-month-old mouse, were used for the measurements in all other genotypes. *Cyp27a1*$^{+/+}$*Cyp46a1*$^{+/+}$ and *Cyp27a1*$^{-/-}$*Cyp46a1*$^{-/-}$ mice were on the C57BL/6J;129S6/SvEv background. *Acat1*$^{+/+}$ and *Acat1*$^{-/-}$ mice were on the C57BL/6J background. Data on *Cyp27a1*$^{+/+}$*Cyp46a1*$^{+/+}$ and *Cyp27a1*$^{-/-}$*Cyp46a1*$^{-/-}$ genotypes are taken from Ref. 27. **, $p < 0.01$; ***, $p < 0.001$ by Student's *t* test. *Black asterisks* and *horizontal lines* indicate the statistical significance for total cholesterol; *gray asterisks* and *horizontal lines* indicate the statistical significance for unesterified cholesterol.

(phospholipids and UC) of vesicular membranes, whereas *para*-phenylenediamine preserves the lipids (neutral lipids such as EC) in droplets (36). Lipid accumulations were found in the *Cyp27a1*$^{-/-}$*Cyp46a1*$^{-/-}$ OS and RPE but not in the *Cyp27a1*$^{+/+}$*Cyp46a1*$^{+/+}$ retina (Fig. 4). These accumulations were in the form of droplets of varied size, from 50 to 300 nm in diameter, present inside and outside the PR cells as singlets or in clusters (Fig. 4, *B* and *C*). The linear track of droplets in some of the *Cyp27a1*$^{-/-}$*Cyp46a1*$^{-/-}$ OS (Fig. 4*D*) could indicate that droplets are formed inside the PR cell and are then expelled into the interphotoreceptor space following membrane disruption. Lipid droplets were also found in the *Cyp27a1*$^{-/-}$*Cyp46a1*$^{-/-}$ RPE, cytosol, and phagosomes (Fig. 4, *F*, *H*, and *I*) but in apparently smaller amounts than in the *Cyp27a1*$^{-/-}$*Cyp46a1*$^{-/-}$ OS. Unlike the OS, the *Cyp27a1*$^{-/-}$*Cyp46a1*$^{-/-}$ RPE contained large semi-electron-lucent areas with content, which included phagosomes, vesicular membranes, and membranous debris (Fig. 4, *F*, *G*, and *I*). Because EC was not detectable in the *Cyp27a1*$^{-/-}$*Cyp46a1*$^{-/-}$ RPE by filipin (Fig. 2*F*), and we had found previously that the *Cyp27a1*$^{-/-}$*Cyp46a1*$^{-/-}$

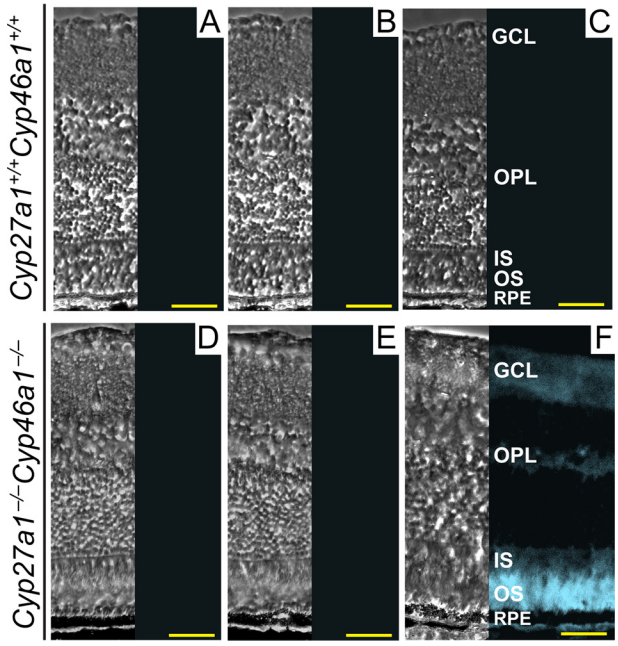

FIGURE 2. **Histochemical detection of retinal EC with filipin.** Filipin is a fluorescent antibiotic that interacts with the 3β-hydroxyl group of UC and other sterols. This allows for the visualization of EC after tissue pretreatment with 70% aqueous ethanol to extract UC followed by cholesterol esterase to release the 3β-hydroxyl group in remaining EC. The *left section* in each *panel* is a phase contrast image, and the *right section* is a histochemistry image. *A* and *D*, control stains for completeness of UC removal. These sections were extracted with ethanol and treated with filipin. *B* and *E*, control stains for background fluorescence. These sections were extracted with ethanol but not treated with filipin or cholesterol esterase. *C* and *F*, stains for EC. These sections were extracted with ethanol and then sequentially treated with cholesterol esterase and filipin. All images are representative: $n = 3$ mice (3–7 months old)/genotype, with one retina from each mouse. *Scale bars*: 100 μm.

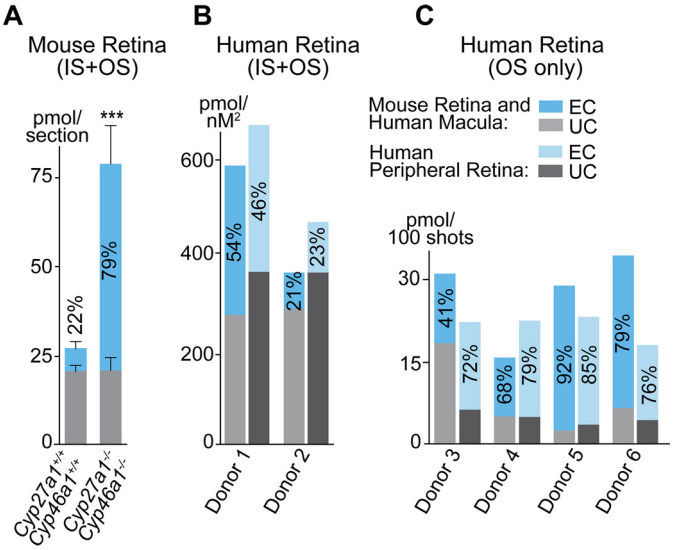

FIGURE 3. **UC and EC content in mouse and human PR cells.** *A*, mouse retina. The results are mean ± S.D. of the measurements in three samples from one retina, each containing four dissectates of the PR area. *B* and *C*, human retina. The results are the mean of the measurements in two samples from one retina, each containing four dissectates (donors 1 and 2), and in one sample, each containing the material from 600–700 laser shots (donors 3–6). The *numbers* inside the *blue bars* are the EC content relative to total cholesterol. Data on total cholesterol in donors 3–6 were published previously in Ref. 5.

RPE may contain focal deposits of UC (27), it is possible that these large semi-electron-lucent areas represent focal deposits of UC. Studies by TEM are supported by our previous light microscopy stains with oil red O, a dye that interacts mainly with neutral lipids and fatty acids. As found from analysis by TEM, the oil red O stains also revealed lipid accumulation in the *Cyp27a1*$^{-/-}$*Cyp46a1*$^{-/-}$ photoreceptors (27).

Localization of Cholesterol-esterifying Enzymes in Mouse Retina—In mammals, cholesterol esterification is carried out by only three enzymes: two isoforms of acyl-coenzyme A:cholesterol acyltransferase (ACAT1 and ACAT2) and lecithin-cholesterol acyltransferase (LCAT) (37–40). Both ACAT isoforms catalyze the esterification of intracellular cholesterol (41, 42), whereas LCAT is a secreted protein, which acts on cholesterol in high-density lipoproteins (43). ACAT1 is ubiquitous, whereas the expression of ACAT2 and LCAT is limited to specific tissues (40, 41, 44). Previously, human and monkey retina was found to contain transcripts for ACAT1 and LCAT but not ACAT2 (45, 46) and also to express LCAT as a protein (47). We investigated whether *Acat2* was also at low abundance in mouse retina. We used qRT-PCR and quantified the expression of *Acat1*, *Acat2*, and *β-actin* in wild type and *Cyp27a1*$^{-/-}$ *Cyp46a1*$^{-/-}$ retinas. In both genotypes, the mean Ct numbers (wild type/*Cyp27a1*$^{-/-}$*Cyp46a1*$^{-/-}$) for each of these proteins were very similar and equal to: *Acat1*, 23.9/23.0; *Acat2*, 35.5/34.9, and *β-actin*, 18.5/18.7. Very high Ct numbers for *Acat2* suggest that in mouse retina, the ACAT2 protein levels are quite small if present at all. Therefore, we investigated the retinal expression of ACAT1 and LCAT only following the assessment of the quality of different anti-ACAT1 antibodies (Fig. 5); the anti-LCAT Ab has been characterized previously (47). In both, *Cyp27a1*$^{+/+}$*Cyp46a1*$^{+/+}$ and *Cyp27a1*$^{-/-}$*Cyp46a1*$^{-/-}$ mice, the signal for ACAT1 was detected mainly in the OS (Fig. 6, *A–C* and *I–K*), consistent with the localization of EC and lipid droplets in the *Cyp27a1*$^{-/-}$*Cyp46a1*$^{-/-}$ retina (Figs. 2*F* and 4*B*) and known post-translational activation of ACAT1 by cholesterol excess (48). Both genotypes, however, had essentially no signal for LCAT in the OS, LCAT immunoreactivity was found only in the GCL and OPL (Fig. 6, *D–F* and *L–N*). Staining with glutamine synthase (GS), a marker for Müller cells, demonstrated that the anti-LCAT staining in the *Cyp27a1*$^{-/-}$ *Cyp46a1*$^{-/-}$ retina is in part due to enzyme expression in Müller cells (Fig. 6, *O* and *P*). Thus, it is probably ACAT1 rather than LCAT that esterifies cholesterol excess in the OS in *Cyp27a1*$^{-/-}$*Cyp46a1*$^{-/-}$ mice.

Retinal Cholesterol Esterification in Acat1$^{-/-}$ *Mice*—These animals were used to determine the ACAT1 contribution to a small pool of EC normally detected in mouse retina (Fig. 1*B*). ACAT1 ablation decreased the retinal content of TC but did not seem to change the retinal content of EC (Fig. 1*B*). These results suggest that under hypo- and normocholesterolemic conditions, ACAT1 makes only minor contributions to cholesterol esterification in mouse retina, and the majority of retinal EC is likely produced by LCAT. Consequently, the amount of retinal EC probably reflects the fraction of cholesterol associated with high-density lipoprotein-like particles, suggested to circulate in the retina and mediate intraretinal cholesterol transport (47).

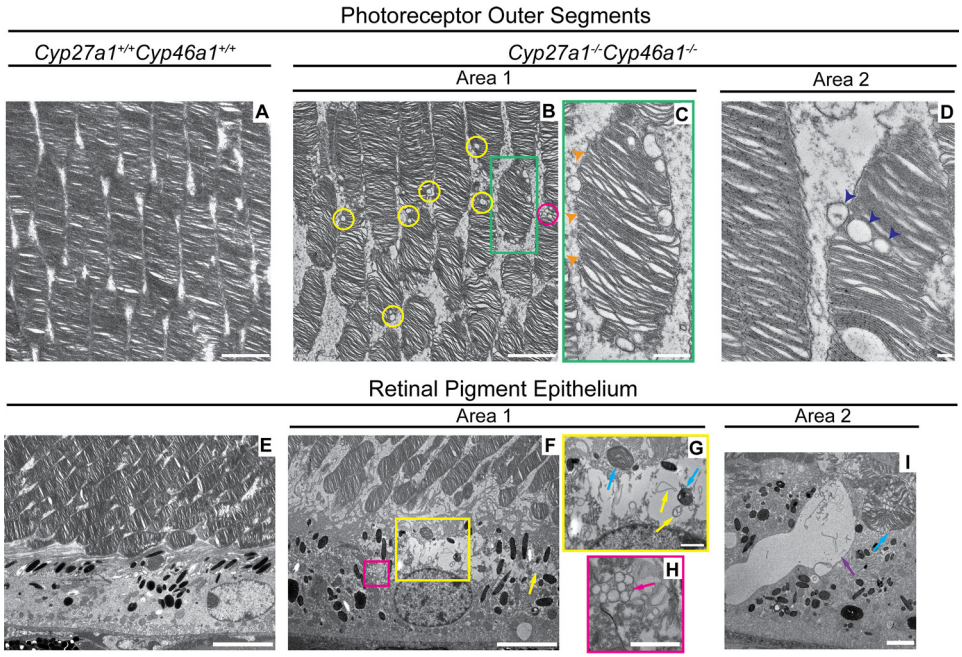

FIGURE 4. **Lipid accumulation in the photoreceptor outer segments and retinal pigment epithelium of *Cyp27a1*$^{-/-}$*Cyp46a1*$^{-/-}$ mice.** Transmission electron micrographs of *Cyp27a1*$^{+/+}$*Cyp46a1*$^{+/+}$ mice (*A* and *E*) and *Cyp27a1*$^{-/-}$*Cyp46a1*$^{-/-}$ mice (*B–D* and *F–I*). *C*, *G*, and *H*, *enlarged images* of the *boxed regions* in *B* and *F*, respectively. *B*, single lipid droplets (*yellow circles*) and a cluster of lipid droplets (*magenta circle*). *C*, absent plasma membrane in the outer segment (*orange arrowheads*). *D*, linear track of lipid droplets (*dark blue arrowheads*) suggesting that these lipid droplets are being expelled from the outer segment. *F–H*, lipid-containing areas with membranous debris and membranous particles (*yellow boxed area* and *yellow arrows*, respectively) or a cluster of lipid droplets (*magenta boxed area* and *magenta arrow*, respectively). *G* and *I*, phagosomes (*blue arrows*), one of which (*I*) contains lipid droplets. *I*, a lipid lake (*purple arrow*). All images are representative: $n = 3$ mice (7 months old)/genotype, with one retina from each mouse. *Scale bars*: *A*, *B*, and *I*, 2 μm; *C*, 0.5 μm; *D*, 0.2 μm; *E* and *F*, 5 μm; *G* and *H*, 1 μm.

Cholesterol Esterification in Human Retina—Mice and humans have differences in their retinal architecture and physiology (49) and the way they handle cholesterol (50). In contrast to mice, the human retina has the macula, a cone-enriched area responsible for high acuity vision, and is dominated by cone cells over rod cells. Because of these peculiarities of the human retina, we used two retinal regions, the macula and the periphery, from donors with no apparent retinal pathology (Table 1). Two retinas, each from a different donor, were characterized for cholesterol content in the PR cells isolated by LCM (Fig. 3*B*). Macular and peripheral retinas from each donor contained a similar relative content of EC (% TC), yet this relative content was very different in the two donors (46–54% and 21–23%) suggesting interdonor variability. A different quality of retinal sections leading to differences in the spatial density of the PR cells precludes interdonor comparisons with respect to absolute cholesterol content. Nevertheless, it seems that human PR cells with a higher TC content have a higher EC content (Fig. 3*B*, compare donor 1 and donor 2), similar to mouse PR cells (Fig. 3*A*, compare *Cyp27a1*$^{+/+}$*Cyp46a1*$^{+/+}$ and *Cyp27a1*$^{-/-}$*Cyp46a1*$^{-/-}$ mice). Four retinas, each from a different donor, were analyzed for the relative EC content in the OS only (Fig. 3*C*). In the macula, the EC content in the OS showed more interdonor variability (from 41 to 92%) than in the peripheral retina (from 68 to 85%). However, the mean relative EC values were similar, 70 and 78%, in macular and peripheral OS, respectively, and higher than those in the whole PR region. The latter finding suggests that the IS contain less EC than the OS.

We next characterized the human retina for expression of ACAT1 and LCAT (Fig. 7). The anti-ACAT1 staining pattern was similar in macular and peripheral retinas (Fig. 7, *A–F*) but different from that in the mouse retina, which seems to express ACAT1 in the OS only (Fig. 6, *C* and *K*). In human retina, the anti-ACAT1 signal was observed in the GCL, the OPL (in the peripheral retina only), the IS, and the basal aspect of the RPE. ACAT1 co-localization with drusen (Fig. 7*F*) provides insight into the origin of EC in this hallmark of AMD. The immunoreactivity for LCAT was very similar in human (Fig. 7, *G–L*) and mouse retina (Fig. 6, *D–F* and *L–N*) with both showing an immunosignal in the GCL and OPL. Moreover, labeling of the Müller cell processes in human retina was similar to that observed in the *Cyp27a1*$^{-/-}$*Cyp46a1*$^{-/-}$ retina (Fig. 6, *O* and *P*) but not the *Cyp27a1*$^{+/+}$*Cyp46a1*$^{+/+}$ retina (Fig. 6, *G* and *H*). Thus, there seem to be both similarities and differences in the way humans and mice esterify retinal cholesterol.

Retinal Manifestations of Cyp27a1$^{-/-}$*Cyp46a1*$^{-/-}$*Acat1*$^{-/-}$ *Deficiency*—The presence of cholesterol excess in the form of EC in the *Cyp27a1*$^{-/-}$*Cyp46a1*$^{-/-}$ OS prompted us to generate *Cyp27a1*$^{-/-}$*Cyp46a1*$^{-/-}$*Acat1*$^{-/-}$ mice to confirm the proposed role of ACAT1 and to investigate the retinal consequences of UC accumulation. We found that EC was virtually absent in the retina of these animals, and the amount of UC was indeed increased in their retina as compared with that in the retina of *Cyp27a1*$^{-/-}$*Cyp46a1*$^{-/-}$ and *Acat1*$^{-/-}$ mice (Fig. 1*C*). This increase, however, was not as high as the increase in TC in the *Cyp27a1*$^{-/-}$*Cyp46a1*$^{-/-}$ retina, indicating that mouse retina does not tolerate a significant increase in UC. The measurements of lathosterol, a general marker of cholesterol biosynthesis (51), showed the same sterol levels in the retina of *Acat1*$^{+/+}$ and *Acat1*$^{-/-}$ mice (76–79 pmol/mg protein in

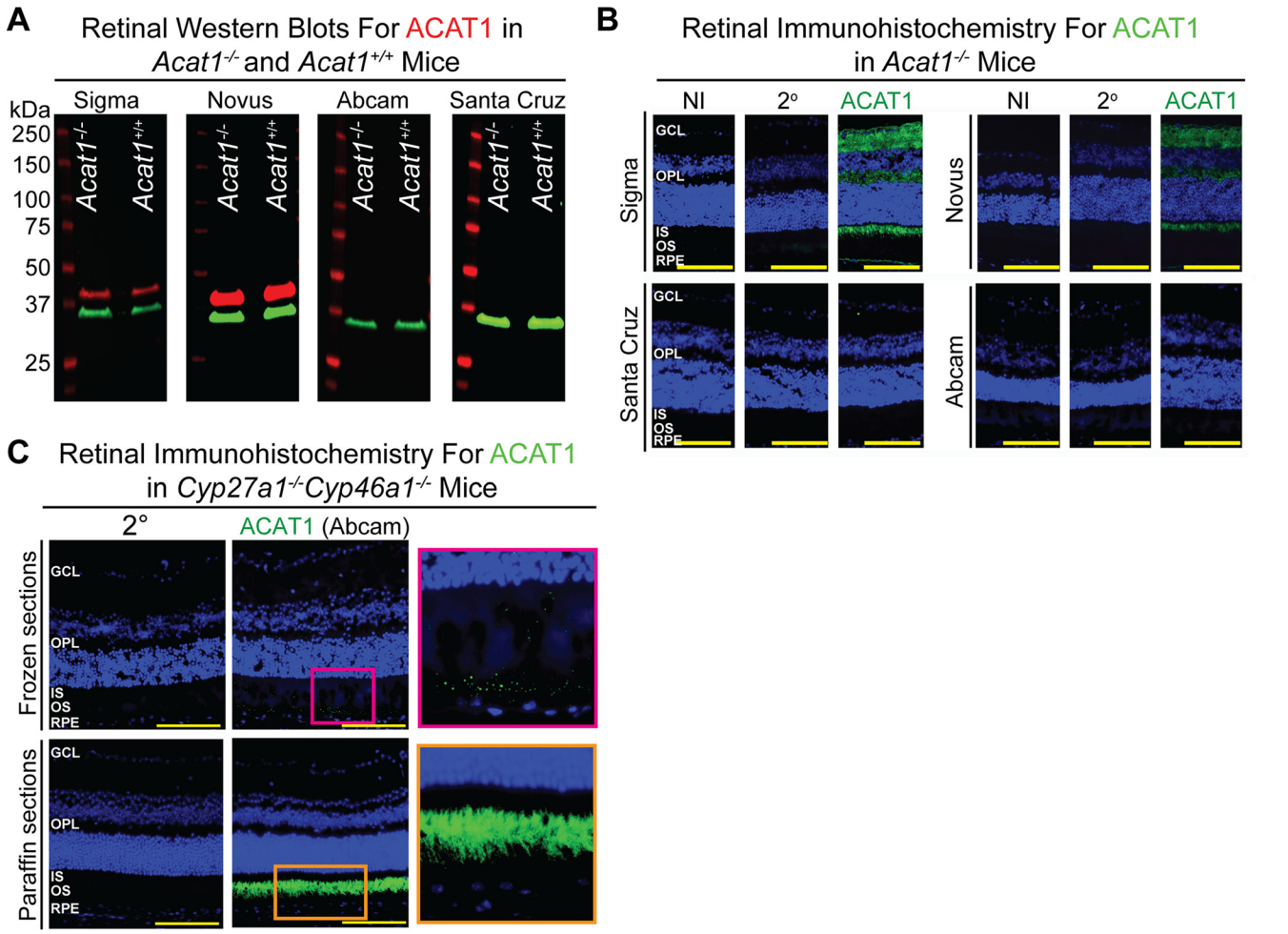

FIGURE 5. **Search for specific ACAT1 antibodies.** *A*, comparison of the specificity of ACAT1 antibodies from different vendors as assessed by Western blotting analysis. Retinal homogenates from *Acat1*$^{-/-}$ (negative control) and *Acat1*$^{+/+}$ mice (3–4 months old) were run side by side on SDS-PAGE. Membranes, after transfer and blocking, were cut and probed separately with primary antibodies from Sigma, Novus, Abcam, and Santa Cruz Biotechnology. The immunoreactive signal for ACAT1 is in *red*, and that for GAPDH (served as a loading control) is in *green*. Primary antibodies from Sigma, Novus, and Santa Cruz Biotechnology showed similar immunoreactivity for ACAT1 in retinal homogenates from *Acat1*$^{-/-}$ and *Acat1*$^{+/+}$ mice and recognized proteins with molecular masses different from that of full size ACAT1 (~64 kDa). Only primary antibody from Abcam did not show any immunoreactivity for ACAT1 in both *Acat1*$^{-/-}$ and *Acat1*$^{+/+}$ retinal homogenates. *B*, comparison of the specificity of anti-ACAT1 antibodies from Sigma, Novus, Santa Cruz Biotechnology, and Abcam as assessed by control stains with the nonimmunized (*NI*) serum and the secondary antibody (*2°*), respectively, and immunohistochemical stains of *Acat1*$^{-/-}$ retinal sections. Nuclei were stained with DAPI (in *blue*). Only primary antibodies from Santa Cruz Biotechnology and Abcam did not show any immunoreactivity for ACAT1. Because the primary antibody from Abcam also did not show any immunoreactivity for ACAT1 in *Acat1*$^{-/-}$ retinal homogenates, this antibody was chosen for further testing on retinal sections from different mouse genotypes. *C*, control stains with secondary antibody and retinal immunolocalization of ACAT1 with primary antibody from Abcam in *Cyp27a1*$^{-/-}$*Cyp46a1*$^{-/-}$ mice (6–8 months old). Nuclei were stained with DAPI (in *blue*). *Enlarged images* of the *boxed regions* are also shown. Only a weak punctate signal was observed in frozen retinal sections, which was mainly localized to the OS with minor punctate immunoreactivity in the IS. Retinal paraffin sections showed a much stronger anti-ACAT1 immunoreactivity, which was localized only to the OS. *Scale bars* 100 μm.

males or females) and a 1.4-fold decrease ($p < 0.01$ and 0.001 for males and females, respectively) in retinal lathosterol levels in the *Cyp27a1*$^{-/-}$*Cyp46a1*$^{-/-}$*Acat1*$^{-/-}$ genotype (54–58 pmol/mg protein in males or females). Thus, the accumulation of UC in the *Cyp27a1*$^{-/-}$*Cyp46a1*$^{-/-}$*Acat1*$^{-/-}$ retina leads to a compensatory down-regulation of cholesterol biosynthesis, thereby further confirming that mouse retina is very sensitive to UC excess, possibly because of its toxicity. Interestingly, the amounts of unesterified retinal cholestanol, the cholesterol biohydrogenation product up-regulated in CYP27A1 deficiency (52), were similarly high in the *Cyp27a1*$^{-/-}$*Cyp46a1*$^{-/-}$ and *Cyp27a1*$^{-/-}$*Cyp46a1*$^{-/-}$*Acat1*$^{-/-}$ genotypes, with 10-fold and 5-fold increases in the retina of *Cyp27a1*$^{-/-}$*Cyp46a1*$^{-/-}$ females and males, respectively (27), and 9- and 6-fold increases in the retina of *Cyp27a1*$^{-/-}$*Cyp46a1*$^{-/-}$*Acat1*$^{-/-}$ females (864 pmol/mg protein) and males (567 pmol/mg protein), respectively. Thus, in contrast to UC, mouse retina can tolerate the accumulation of unesterified cholestanol, a sterol that is structurally very similar to cholesterol.

Cyp27a1$^{-/-}$*Cyp46a1*$^{-/-}$*Acat1*$^{-/-}$ mice were next evaluated by ultra-high resolution spectral domain optical coherence tomography (SD-OCT) for SDD, which can be detected by this imaging modality (15). The retina of 6- and 9-week-old *Cyp27a1*$^{-/-}$*Cyp46a1*$^{-/-}$*Acat1*$^{-/-}$ mice showed changes on SD-OCT; the hyporeflective band separating the hyperreflective OS and RPE bands was not clearly seen, and the OS band became broader and indistinct (Fig. 8, *A* and *C*). The OS broadening appeared to be more pronounced at 9 weeks of age than at

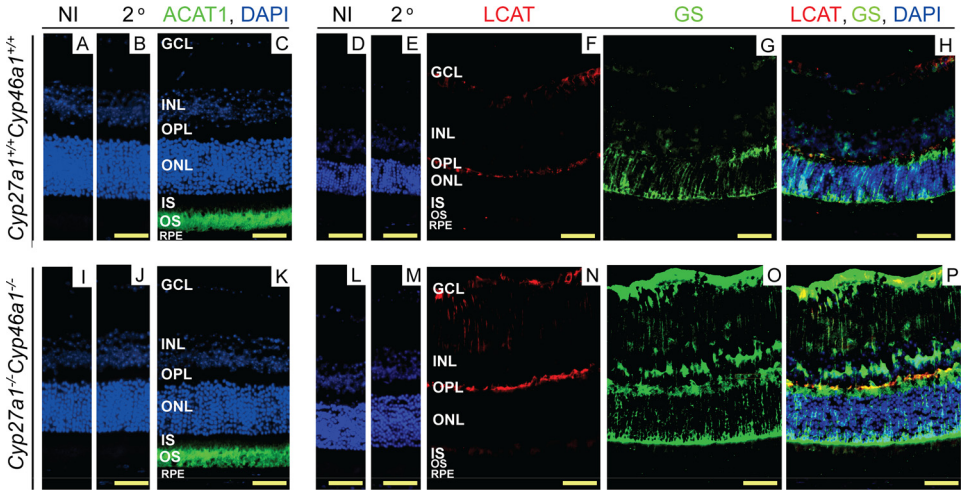

FIGURE 6. **Immunolocalizations of ACAT1 and LCAT in mouse retina.** *A*, *D*, *I*, and *L*, control stains with nonimmunized (*NI*) serum; and *B*, *E*, *J*, and *M*, secondary (*2°*) antibody. Nuclei were stained with DAPI (in *blue*). *C* and *K*, stains for ACAT1 (in *green*); *F* and *N*, LCAT (in *red*); and *G* and *O*, glutamine synthase (in *green*). *H* and *P*, *overlays* of *F* and *G* and *N* and *O*, respectively. Immunoreactivity for ACAT1 and LCAT was detected with Alexa Fluor 647-conjugated secondary antibody and that for GS with Alexa Fluor 488 secondary antibody. All images are representative: $n = 3$ mice (6–8 months old)/genotype, with one retina from each mouse. *Scale bars*: 50 μm.

TABLE 1
Demographic information on the donors whose retinas were used in the present study

Donor ID	Age	Gender
	year	
1[a]	82	M
2[a]	74	M
3[b]	59	M
4[b]	64	M
5[b]	78	M
6[b]	85	M
PM024[c]	84	F
PM032[c]	68	M
PM037[c]	61	M

[a] Retinal sections from these donors were used for cholesterol quantifications in the photoreceptors as well as immunohistochemistry.
[b] Retinal sections from these donors were provided by Dr. Curcio, University of Alabama at Birmingham, and used for cholesterol quantifications in the photoreceptor outer segments.
[c] Retinal sections from these donors were used for immunohistochemistry.

6 weeks of age, suggesting an age-dependent process reminiscent of that reported for stage 1 SDD (Fig. 8*G*) (15). The manifestations of this process were consistent with the young age of the investigated animals and were different from the changes in the *Cyp27a1*$^{-/-}$*Cyp46a1*$^{-/-}$ retina (Fig. 8*E*), which affected the IS/OS interface. The progressive process in the *Cyp27a1*$^{-/-}$*Cyp46a1*$^{-/-}$*Acat1*$^{-/-}$ retina was further confirmed by SD-OCT examination of mice at 5.5 months of age. This time point revealed retinal degeneration as indicated by a decrease in the thickness of the whole retina as well as the outer retinal region defined by the external limiting membrane and including the RPE (Fig. 9, *A*, *B*, *G*, and *H*). Retinal degeneration was also indicated by a patchy pattern of the rod opsin immunolabeling with a shortened OS length (Fig. 9*J*) and a significant number of the photoreceptor apoptotic cells detected by TUNEL staining (Fig. 9*K*), which were absent in the *Cyp27a1*$^{+/+}$*Cyp46a1*$^{+/+}$*Acat1*$^{+/+}$ retina (Fig. 9*E*) and the *Cyp27a1*$^{-/-}$*Cyp46a1*$^{-/-}$ retina (not shown). Filipin staining demonstrated that UC accumulates in the *Cyp27a1*$^{-/-}$*Cyp46a1*$^{-/-}$*Acat1*$^{-/-}$ OS (Fig. 9*D*), suggesting that it could be the UC excess that triggers the outer segment degeneration and photoreceptor cell apoptosis. Comprehensive characterization of *Cyp27a1*$^{-/-}$*Cyp46a1*$^{-/-}$*Acat1*$^{-/-}$ mice will be reported elsewhere.

Discussion

The major finding of the present work is that in mice with retinal hypercholesterolemia induced by ablation of the two major retinal cholesterol-eliminating hydroxylases, cholesterol accumulates and is esterified in the OS, the retinal layer that normally has the lowest cholesterol content. This finding is consistent with previous data in the field that suggest the mechanism for this accumulation and esterification. Specifically, we found that both human and mouse OS have a unique cholesterol maintenance among retinal cells because they lack the major proteins involved in cholesterol biosynthesis (HMGCR), uptake (LDLR), metabolism (CYPs 46A1 and 27A1), efflux (ABCA1 and ABCG1), and transcriptional regulation (SREBP, SCAP, INSIG, and LXR) (3, 4). Others also have shown that the expression of lysosomal cholesterol ester hydrolase, the enzyme that de-esterifies cholesterol esters, is limited to the RPE only (53). Unlike the OS, the IS, which is the nearby PR compartment, expresses many of cholesterol-related proteins in both humans and mice (3, 4). Hence, we suggested that the OS lack the major pathways of cholesterol input and output to minimize their cholesterol content and thereby prevent cholesterol loss in the retina from daily phagocytosis. We also proposed that the OS obtain cholesterol from the IS, either by passive diffusion or intracellular cholesterol transport (3). The IS eliminate cholesterol, at least in part, via hydroxylation catalyzed by CYP27A1, which is highly abundant in this layer (54). Accordingly, in *Cyp27a1*$^{-/-}$*Cyp46a1*$^{-/-}$ mice with nonfunctional CYP27A1, cholesterol excess is not eliminated from the IS but rather is likely delivered to the OS, where it is accumulated and activates ACAT1, which we have demonstrated to be expressed in the OS (Fig. 6, *C* and *K*). Thus, it is a simultaneous lack of CYP27A1 and retinal cholesterol ester hydrolase, yet the presence of ACAT1 that probably contributes to cholesterol accu-

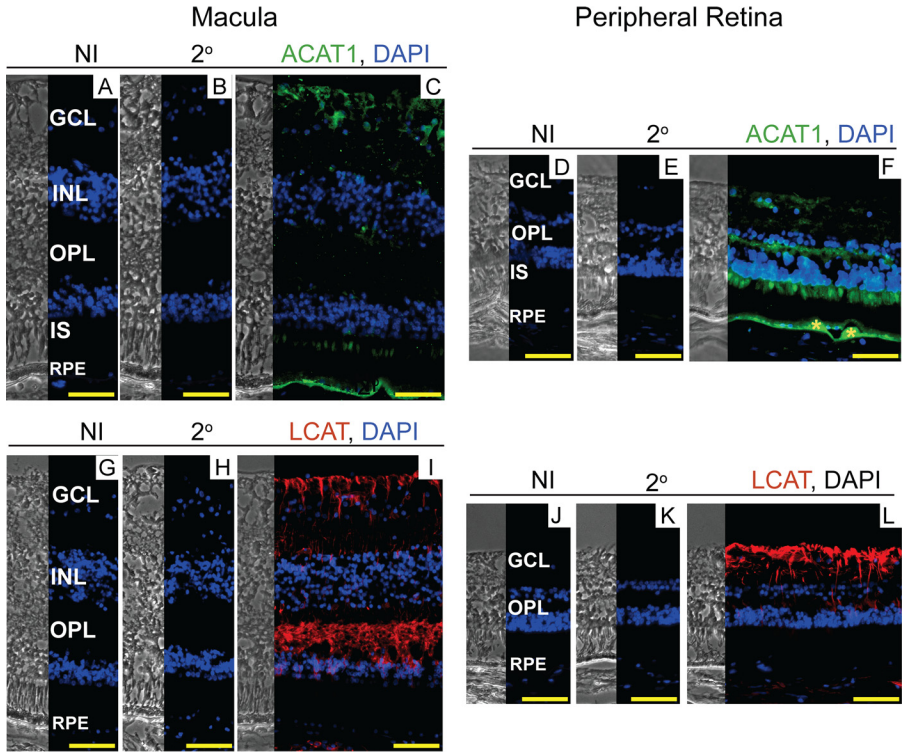

FIGURE 7. **Immunolocalizations of ACAT1 and LCAT in human retina.** The *left* and *right sections* in each *panel* are phase contrast images and histochemistry images, respectively. *A*, *D*, *G*, and *J*, control stains with nonimmunized (*NI*) serum; and *B*, *E*, *H*, and *K*, secondary (*2°*) antibody. Nuclei were stained with DAPI (in *blue*). *C* and *F*, stains for ACAT1 (in *green*); and *I* and *L*, LCAT (in *red*). Immunoreactivity was detected by Alexa Fluor 647-conjugated secondary antibody. *F*, *yellow asterisks* indicate drusen. All images are representative ($n = 5$ donors). Sections of the macular and peripheral retina are from the same donor. *Scale bars*: 50 μm.

mulation and esterification in the *Cyp27a1*$^{-/-}$*Cyp46a1*$^{-/-}$ OS.

In contrast, in animals with normal CYP27A1 activity, the contribution of ACAT1 to retinal cholesterol esterification is only minor, if any at all (Fig. 1*B*), likely because ACAT1 activity is controlled by cholesterol availability, *i.e.* intracellular accumulation (48), which is prevented by CYP27A1. We suggest that cholesterol esterification in normo- or hypocholesterolemic mouse retina mostly reflects the esterification of extracellular cholesterol and is likely carried out by LCAT (Table 2). Consistent with this explanation is the lack of cholesterol esterification in the *Cyp27a1*$^{-/-}$*Cyp46a1*$^{-/-}$*Acat1*$^{-/-}$ retina (Fig. 1*C*), because UC accumulates in the OS and is not likely to be available for extracellular esterification by LCAT.

Insights into the pathophysiologic relevance of intracellular cholesterol esterification were also obtained. In mice, ACAT1-mediated cholesterol esterification was found to be protective for many cell types, as UC excess could be toxic to cells (55). This was the case for mouse brain and skin cells in the setting of hypercholesterolemia (56, 57) and the blood vessels of the systemic circulation in *Ldlr*$^{-/-}$ mice (58). Our data indicate that in the retina, the significance of cholesterol esterification could be cell-specific and both beneficial and detrimental. By 6 months of age, the *Cyp27a1*$^{-/-}$*Cyp46a1*$^{-/-}$ retina had significant vascular abnormalities, macrophage activation, and increased oxidative stress as well as impaired function of the *Cyp27a1*$^{-/-}$ *Cyp46a1*$^{-/-}$ PR cells, as indicated by their altered electrical responses (27). In contrast, *Cyp27a1*$^{-/-}$*Cyp46a1*$^{-/-}$*Acat1*$^{-/-}$ mice do not appear to have retinal vascular abnormalities, as assessed by fluorescein angiography (data are not shown), even at 5.5 month of age. However, they show photoreceptor degeneration (Fig. 9, *A–C*, *E*, *G–I*, and *K*), which is not present in *Cyp27a1*$^{-/-}$*Cyp46a1*$^{-/-}$ mice (27). These retinal phenotypes suggest that the esterification of cholesterol excess due to the ablation of the cholesterol-metabolizing enzymes is detrimental for the retinal vasculature but is protective, at least in part, for photoreceptor cells. It still remains to be clarified whether the impaired PR function in *Cyp27a1*$^{-/-}$*Cyp46a1*$^{-/-}$ mice is due to other retinal abnormalities and/or the accumulation of lipid droplets in the OS; the latter may affect PR morphology.

Our second major finding is that EC is highly abundant in human OS, as revealed by coupling LCM to GC-MS, a technically advanced approach that we developed (Fig. 3*C*). EC, normally present in only small amounts (~13%) in human retina (32), has never been localized to retinal layers because its amounts are below the limits of detection by filipin (13). We found EC in human OS, raising the question of whether this EC represents retinal cholesterol esterified by LCAT on lipoprotein particles in the photoreceptor matrix or by ACAT1 intracellularly. Despite differences in retinal architecture and physiology, humans and mice appear to have similar retinal LCAT expression. Yet their ACAT1 expression appears to be different (Figs. 6 and 7). Because in wild type mice, retinal cholesterol seems to be mainly esterified by LCAT (Fig. 1*B*), it is conceivable that under normal conditions, cholesterol esterification by LCAT is probably the major mechanism of retinal EC formation in both humans and mice. However, under the conditions of retinal hypercholesterolemia, the two species may process retinal cholesterol excess differently as they have different capacities to esterify cholesterol by ACAT1 (Table 2). Mice

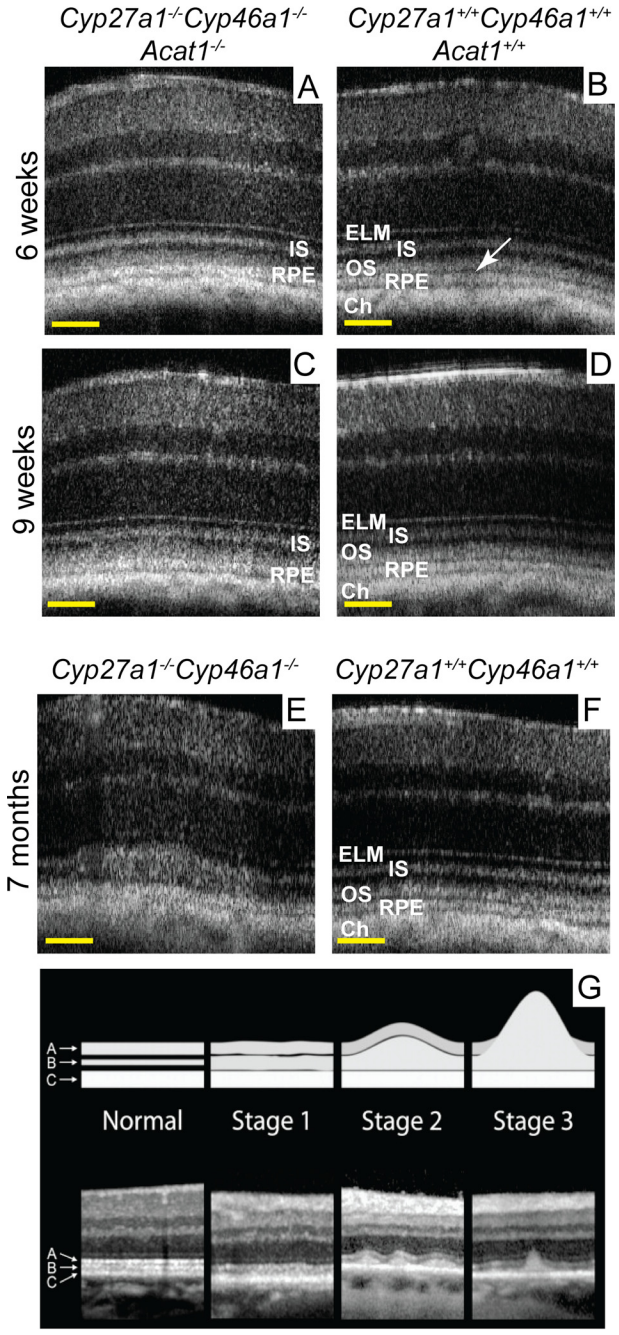

FIGURE 8. **Retinal abnormalities in genetically modified mice.** Retinal SD-OCT of *Cyp27a1*$^{-/-}$*Cyp46a1*$^{-/-}$*Acat1*$^{-/-}$ (*A* and *C*), *Cyp27a1*$^{+/+}$*Cyp46a1*$^{+/+}$ *Acat1*$^{+/+}$ (*B* and *D*), *Cyp27a1*$^{-/-}$*Cyp46a1*$^{-/-}$ (*E*), and *Cyp27a1*$^{+/+}$ *Cyp46a1*$^{+/+}$ (*F*) mice. The same mouse was assessed in *A* and *C*. The *white arrow* in *B* points to the hyporeflective band almost absent in *A* and *C*. All images are representative ($n = 3$ mice/genotype). *G*, stages of subretinal drusenoid formation in human retina taken with permission from Zweifel *et al*. (15). *Scale bars*: *A–F*, 100 μm.

express ACAT1 in the OS and therefore could esterify cholesterol excess in the OS by ACAT1. Conversely, humans do not seem to express ACAT1 in the OS; hence, their capacity for cholesterol esterification in the OS is either absent or very limited as inferred from studies in other cell types. Indeed, in macrophages, up to 10–15% of ACAT1 can be expressed in plasma membranes (59). Consequently, in human OS, a small portion of ACAT1 could be associated with the plasma membranes and PR disks derived from these membranes but be below the limits of detection by immunohistochemistry. In macrophages, ACAT1 also has been shown to be translocated to the sites of increased cholesterol load via the vesicles rich in ACAT1 that are derived from the endoplasmic reticulum (60–63). Similarly, in the human retina, ACAT1 could be delivered to the OS in the vesicles derived from the endoplasmic reticulum of the IS where this enzyme appears to be expressed. Thus, studies on other cell types suggest that cholesterol excess in human OS could be esterified in part by ACAT1, but this esterification will be limited by low enzyme availability.

If cholesterol esterification by LCAT is the major mechanism of retinal EC formation in both humans and mice, and EC is accumulated in the OS, why does this layer lack significant immunoreactivity for LCAT in both species (Figs. 6*F* and 7, *I* and *L*)? This could be due to the association of LCAT with lipoprotein particles and hence enzyme "dilution" in the photoreceptor matrix as compared with when enzyme is expressed intracellularly. Also, we did not reproduce the LCAT immunolocalization to the OS shown in the previous study (47), although we used the same anti-LCAT Ab vendor and an even lower dilution (1:70 *versus* 1:1000). Additional investigations are required to clarify the contribution of lipoprotein EC to total EC in the OS and the reason for the discrepancies in LCAT localization for different species and laboratories. Both studies, however, agree on LCAT immunolocalization to the GCL and in part to Müller cells (Fig. 7, *I* and *L*), which provides an important insight into the potential function of these cells. LCAT and apolipoprotein E, also expressed by Müller cells (64–67), are the two major proteins necessary for lipoprotein particle biogenesis. Hence, Müller cells in the retina could have a role similar to that of brain astrocytes, which are believed to produce the majority of brain cholesterol and express apolipoprotein E along with LCAT for cholesterol delivery to brain neurons (47, 68, 69). Of importance could be our finding that LCAT staining in the *Cyp27a1*$^{-/-}$*Cyp46a1*$^{-/-}$ retina seemed to be more pronounced in Müller cell processes than in the *Cyp27a1*$^{+/+}$ *Cyp46a1*$^{+/+}$ retina (Fig. 6, *H* and *P*). This could reflect an increased need for cholesterol esterification on the lipoprotein particles under the condition of retinal hypercholesterolemia. It seems that not only intracellular but also extracellular cholesterol esterification is increased in the *Cyp27a1*$^{-/-}$ *Cyp46a1*$^{-/-}$ retina.

On the basis of our results, we put forward the hypothesis that impaired ACAT1 activity could be a factor underlying the development of SDD in humans. First, human *ACAT1* or *SOAT1* gene (Mendelian Inheritance in Man database 102642) is highly polymorphic and has frequent mRNA- and protein-altering variants, for which the functional significance is currently unknown. Second, SDD are associated with increased mortality rate, which could be a manifestation of a systemic condition (25, 70). If humans indeed have only limited ability to esterify cholesterol in the OS by ACAT1, then the polymorphism-determined impairment in ACAT1 activity could have a significant effect on cholesterol homeostasis in human OS. We envision that this impairment will predispose the polymorphism carriers to SDD because UC excess will ultimately be expelled from their OS into the subretinal space and deposited

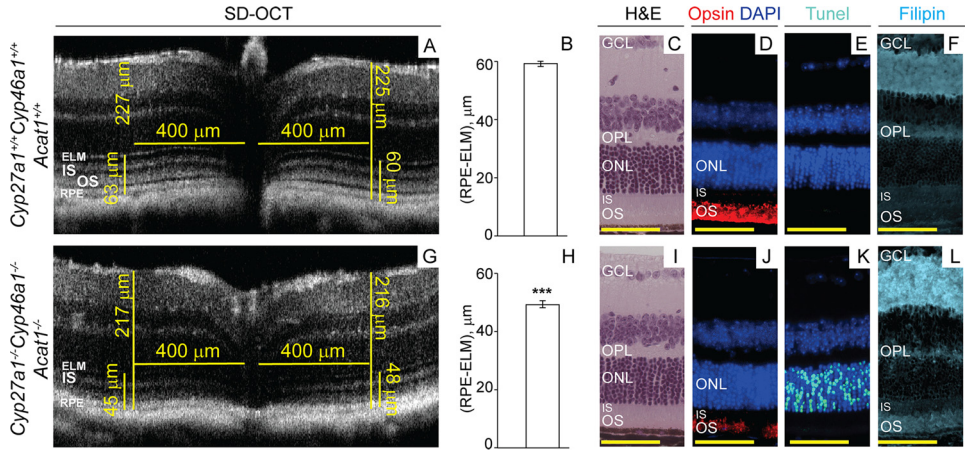

FIGURE 9. **Retinal manifestations of *Cyp27a1*$^{-/-}$*Cyp46a1*$^{-/-}$*Acat1*$^{-/-}$ deficiency.** *A* and *G*, representative ($n = 6$ eyes from 3 mice/genotype) retinal SD-OCT of 5.5-month-old *Cyp27a1*$^{+/+}$*Cyp46a1*$^{+/+}$*Acat1*$^{+/+}$ and *Cyp27a1*$^{-/-}$*Cyp46a1*$^{-/-}$*Acat1*$^{-/-}$ mice, respectively, showing in the latter a panretinal decrease of the whole retinal thickness (*long vertical bars*) and the thickness of the RPE-external limiting membrane (*ELM*) region (*short vertical bars*). Both *Cyp27a1*$^{+/+}$*Cyp46a1*$^{+/+}$ (C57BL/6J;129S6/SvEv background) and *Acat1*$^{+/+}$ mice (C57BL/6J strain) have the same retinal thickness. *B* and *H*, the quantifications of the thickness of the RPE-ELM region. The results are mean ± S.D. of the measurements in the nasal and temporal retina (400 μm from the optic nerve) from 6 eyes/3 mice/genotype. ***, $p < 0.001$ by Student's *t* test. *C–F* and *I–L*, animals in *A* and *B*, respectively, were then used for evaluations by H&E histology (*C* and *I*) and anti-rhodopsin (*D* and *J*, in *red*), TUNEL (*E* and *K*, in *cyan*), and UC stains by filipin (*F* and *L*, in *cyan*). Nuclei were stained with DAPI (in *blue*). Immunoreactivity was detected by Alexa Fluor 555-conjugated secondary antibody. All images are representative ($n = 3$ mice/genotype). *Scale bars*: 50 μm.

TABLE 2

Proposed contributions of LCAT and ACAT1 to cholesterol esterification in the retina

+, minor contribution; +++, significant contribution.

Cholesterol-esterifying enzyme	Hypocholesterolemic retina	Normocholesterolemic retina		Hypercholesterolemic retina	
	Mice	Mice	Humans	Mice	Humans
LCAT	+++	+++	+++	+++	+++
ACAT1	+	+	+	+++	+

outside the cell. We suggest that SDD-affected individuals should be tested for the polymorphisms in *ACAT1*. Furthermore, we suggest that ACAT1 localization in the OS in mice prevents the development of SDD in this species. We have provided support for this interpretation by generating *Cyp27a1*$^{-/-}$*Cyp46a1*$^{-/-}$*Acat1*$^{-/-}$ animals, which have progressive changes on SD-OCT similar to those characteristic of early stage SDD, UC accumulation in the OS, and retinal degeneration (Figs. 8 and 9).

In summary, we studied cholesterol esterification in the mouse and human retina and found that this process could be of particular importance for PR cells under an increased load of retinal cholesterol. We established that mice and humans have both similarities and interspecies differences in retinal cholesterol esterification and that in humans, cholesterol esterification by ACAT1 could be of clinical significance. We suggest that polymorphisms in *ACAT1* could be a risk factor for the SDD biogenesis and put forward a testable hypothesis explaining the etiology of SDD, the formation of which is currently poorly understood. We began to test this hypothesis by generating a genetically modified mouse. The data obtained provide substantial new mechanistic insights into retinal cholesterol maintenance and bring attention to a previously unappreciated but important cholesterol-related pathway in the retina.

Experimental Procedures

Animals—*Cyp27a1*$^{-/-}$*Cyp46a1*$^{-/-}$ mice on a mixed strain background (C57BL/6J;129S6/SvEv) were generated previously in this laboratory (27). They no longer contained the *Crbl*^{rd8} mutation that was bred out from our colony. *Acat1*$^{-/-}$ mice (71) were obtained from the laboratory of Dr. T. Y. Chang (Dartmouth College, Hanover, NH) and were free of the *Crbl*^{rd8} mutation. They were rederived on the C57BL/6J strain and crossed with *Cyp27a1*$^{-/-}$*Cyp46a1*$^{-/-}$ mice to generate *Cyp27a1*$^{-/-}$*Cyp46a1*$^{-/-}$*Acat1*$^{-/-}$ mice. All animals were maintained on a standard 12-h light (~10 lux)-dark cycle and were provided standard rodent chow and water provided *ad libitum*.

Sample Preparation and Sterol Quantifications—Sample processing and GC-MS analyses were as described (29). Mouse retinas were isolated as described (27). Samples from the LCM were obtained as follows. Cryosections of the retina (20-μm thick for mouse retina and human retina from donors 1 and 2 and 10-μm thick for donors 3–6) were placed on slides (PEN membrane glass slides from Arcturus Bioscience for mouse retina and human retina from donors 1 and 2 and Superfrost Plus slides from Fisher Scientific for donors 3–6). The slides were rinsed in purified, distilled water for 5 min and placed in a vacuum desiccator. Slides were dried for 48 h and kept in the vacuum desiccator until dissection by LCM. Mouse microsections and microsections from donors 1 and 2 were isolated by a Leica LMD7000 laser microdissection system (Leica Microsystems). The area for microdissection was first defined by using the ×20 magnification objective. The laser beam was then precisely steered by the prisms along the defined area, and the dissectate fell in a collection tube. For each mouse genotype,

three samples from one retina, each containing four dissectates of the whole PR area (both IS and OS), were processed for TC and UC quantifications. For donors 1 and 2, two samples/donor, each containing four 600,000–900,000-μm^2 dissectates, were processed for TC and UC quantifications. Microsections from donors 3–6 were isolated by a PixCell IIe LCM system (Applied Biosystems) and CapSure Macro LCM caps (Applied Biosystems). For these donors, one sample/donor, each containing the material from 600–700 sequential laser shots, was processed for TC and UC quantifications.

Staining for EC—This was carried out as described using filipin (3).

TEM and SD-OCT—These procedures were as described (72, 73) and utilized a 1200EX transmission electron microscope (JEOL Ltd.) and the 840HHP SD-OCT system (Bioptigen). Tissue fixation for TEM was as described (36) and included sequential incubations in 3% glutaraldehyde in 0.1 M sodium cacodylate buffer, pH 7.4, 1% OsO_4 in the same buffer, 1% tannic acid in 0.05 M sodium cacodylate, pH 7.4, and 1% *para*-phenylenediamine in 70% ethanol.

Western Blotting—Two retinas from each of three mice of the same genotype were pooled and homogenized manually in 0.15 ml of lysis buffer (50 mM Tris, pH 8.0, 150 mM NaCl, 5 mM EDTA, 1% Nonidet P-40, 0.1% SDS, and cOmplete EDTA-free protease inhibitor mixture from Roche). Retinal homogenates were incubated on ice for 30 min followed by centrifugation at 12,000 × *g* for 15 min at 4 °C. The supernatant was used for SDS-PAGE (30 μg protein/lane) followed by Western blotting, which was performed as described (4) except 0.1% Tween 20 was used in both blocking and washing buffers. Proteins were visualized with the following primary Abs: rabbit anti-ACAT1 from Sigma (HPA004428, dilution 1:1,000), rabbit anti-ACAT1 from Novus (NBP1-89285, dilution 1:200), goat anti-ACAT1 from Santa Cruz Biotechnology (sc-161307, dilution 1:100), and rabbit anti-ACAT1 from Abcam (ab168342, dilution 1:200). The secondary Abs were goat anti-rabbit IRDye 680RD (926-68071, Li-Cor, dilution 1:5,000) or donkey anti-goat IRDye 680RD (925-68074, Li-Cor, dilution 1:5,000). Membranes were also incubated with primary Ab against GAPDH, which was used as a loading control (ab9484, Abcam, dilution 1:5,000) and secondary goat anti-mouse IRDye 800CW Ab (926-32210, Li-Cor, dilution 1:5,000). Membranes were imaged using the Odyssey infrared imaging system (Li-Cor).

Immunohistochemistry—The preparation of frozen and paraffin retinal sections was as described (3, 27, 72), except mice underwent cardiac perfusion with 30 ml of phosphate-buffered saline to remove blood from the retina. Prior to immunohistochemistry, paraffin sections were deparaffinized followed by heat-induced antigen retrieval in a microwave three times for 6 min with 10 mM sodium citrate buffer, pH 6.0, containing 0.05% Tween 20. Subsequent steps were the same for frozen and paraffin sections (27), except the blocking buffer for paraffin sections contained 10% goat serum as compared with 5% goat serum used to block the frozen sections. The dilution and source of primary Ab for the stains were as follows: 1:50 for rabbit anti-ACAT1 (ab168342, Abcam), 1:70 for rabbit anti-LCAT (ab64458, Abcam), 1:100 for rabbit anti-GS (ab73593, Abcam), and 1:1,000 for mouse anti-rhodopsin Ab B6–30 (from the K. Palczewski laboratory) (74). Anti-ACAT1 and anti-LCAT Abs were visualized with goat anti-rabbit Alexa Fluor 647 secondary Ab (111-605-144, Jackson ImmunoResearch Laboratories), whereas anti-GS and anti-rhodopsin Abs were detected with donkey anti-rabbit Alexa Fluor 488 (A11008, Invitrogen) and goat anti-mouse Alexa Fluor 555 secondary Abs (A21424, Life Technologies), respectively. Both secondary Abs were diluted 1:200.

For the preliminary testing shown in Fig. 5*B*, the dilution of primary Ab was 1:50 for rabbit anti-ACAT1 (Abcam), 1:200 for rabbit anti-ACAT1 (Sigma), 1:200 for goat anti-ACAT1 (Santa Cruz Biotechnology), and 1:50 for rabbit anti-ACAT1 (Novus). Primary Abs from Sigma, Abcam, and Novus were visualized with goat anti-rabbit Alexa Fluor 647 secondary Ab (111-605-144, Jackson ImmunoResearch Laboratories) used at a 1:200 dilution. Primary Ab from Santa Cruz Biotechnology was visualized with donkey anti-goat Alexa Fluor 647 Ab (705-605-147, Jackson ImmunoResearch Laboratories) and also was used at a 1:200 dilution. Slides were imaged on an inverted microscope (DMI6000 B, Leica Microsystems) using a Retiga EXi Fast camera (QImaging).

TUNEL—This staining was carried out using a commercially available kit (G3250, Promega) according to the manufacturer's manual. The only exception was the use of 0.3% Triton X-100 in PBS instead of proteinase K for section permeabilization.

qRT-PCR—Total RNA (1 μg) was converted to cDNA by SuperScript III reverse transcriptase (Invitrogen) and used for qRT-PCR conducted on a LightCycler 480 instrument (Roche). The sequences of the primers for gene quantifications were taken from qPrimerDepot, a primer database for qRT-PCR (75). PCR reactions were performed in triplicate and normalized to β-actin.

Statistics—Data represent the mean ± S.D. Comparisons between the groups were made using Student's *t* test assuming a two-tailed distribution, with statistical significance being defined as *, $p \leq 0.05$; **, $p \leq 0.01$; and ***, $p \leq 0.001$. All histo- and immunohistochemistry images are representative of observations made in multiple sections from the retinas of 3–5 different mice or human donors. The statistics for other methods are given either in the previous sections or in the figure legends.

Study Approval—All animal procedures were approved by the Case Western Reserve University Institutional Animal Care and Use Committee and conformed to recommendations of the American Veterinary Association Panel on Euthanasia and the Association for Research in Vision and Ophthalmology. Our human tissue use conformed to the Declaration of Helsinki and was approved as the "Not Human Subjects" research by the Institutional Review Board at Case Western Reserve University. Eyes from donors 1 and 2 were obtained from de-identified individuals from the Cleveland Eye Bank (now Eversight) following written informed consent of the respective families. De-identified retinal sections from donors 3–6 were provided by Dr. C. Curcio (University of Alabama, Birmingham) and also represented the Not Human Subjects research. Only eyes with no apparent retinal pathology were used, as assessed by the examination of post-mortem fundus photographs by a fellowship-trained retina-vitreous specialist following an initial gross inspection of the posterior pole under the dissecting microscope with ×3 magnification.

Author Contributions—A. S., N. M., and T. D. conducted experiments and acquired and analyzed the data. B. A. analyzed the data, and I. A. P. designed experiments, analyzed the data, and wrote the manuscript.

Acknowledgments—We thank the former members of the Pikuleva laboratory, Dr. Saida Omarova and Dr. Casey Charvet, for isolating the OS from donors 3–6; Dr. Cristine Curcio (University of Alabama at Birmingham) for providing retinal sections for these donors; Dr. Krzysztof Palczewski (Case Western Reserve University) for providing the anti-rhodopsin antibodies B6–30; and the Visual Sciences Research Center Core Facility (supported by National Institutes of Health Grant P30 EY11373) for assistance with mouse breeding (Heather Butler and Kathryn Franke), animal genotyping (John Denker), tissue sectioning (Cathy Doller), and microscopy (Dr. Scott Howell). We are also grateful to Dr. Hisashi Fujioka of the Case EM core facility and Dr. Patrick Leahy of the Case LCM core facility.

References

1. Swaroop, A., Kim, D., and Forrest, D. (2010) Transcriptional regulation of photoreceptor development and homeostasis in the mammalian retina. *Nat. Rev. Neurosci.* **11,** 563–576
2. Jayakody, S. A., Gonzalez-Cordero, A., Ali, R. R., and Pearson, R. A. (2015) Cellular strategies for retinal repair by photoreceptor replacement. *Prog. Retin. Eye Res.* **46,** 31–66
3. Zheng, W., Reem, R. E., Omarova, S., Huang, S., DiPatre, P. L., Charvet, C. D., Curcio, C. A., and Pikuleva, I. A. (2012) Spatial distribution of the pathways of cholesterol homeostasis in human retina. *PloS One* **7,** e37926
4. Zheng, W., Mast, N., Saadane, A., and Pikuleva, I. A. (2015) Pathways of cholesterol homeostasis in mouse retina responsive to dietary and pharmacologic treatments. *J. Lipid Res.* **56,** 81–97
5. Pikuleva, I. A., and Curcio, C. A. (2014) Cholesterol in the retina: the best is yet to come. *Prog. Retin. Eye Res.* **41,** 64–89
6. Boesze-Battaglia, K., Hennessey, T., and Albert, A. D. (1989) Cholesterol heterogeneity in bovine rod outer segment disk membranes. *J. Biol. Chem.* **264,** 8151–8155
7. Boesze-Battaglia, K., and Albert, A. D. (1990) Cholesterol modulation of photoreceptor function in bovine retinal rod outer segments. *J. Biol. Chem.* **265,** 20727–20730
8. Albert, A. D., and Boesze-Battaglia, K. (2005) The role of cholesterol in rod outer segment membranes. *Prog. Lipid Res.* **44,** 99–124
9. Bok, D., and Young, R. W. (1979) *Phagocytic Properties of the Retinal Pigment Epithelium*, Harvard University Press, Cambridge, MA
10. Pascolini, D., Mariotti, S. P., Pokharel, G. P., Pararajasegaram, R., Etya'ale, D., Négrel, A. D., and Resnikoff, S. (2004) 2002 global update of available data on visual impairment: a compilation of population-based prevalence studies. *Ophthalmic Epidemiol.* **11,** 67–115
11. Curcio, C. A., Millican, C. L., Bailey, T., and Kruth, H. S. (2001) Accumulation of cholesterol with age in human Bruch's membrane. *Invest. Ophthalmol. Vis. Sci.* **42,** 265–274
12. Curcio, C. A., Presley, J. B., Malek, G., Medeiros, N. E., Avery, D. V., and Kruth, H. S. (2005) Esterified and unesterified cholesterol in drusen and basal deposits of eyes with age-related maculopathy. *Exp. Eye Res.* **81,** 731–741
13. Oak, A. S., Messinger, J. D., and Curcio, C. A. (2014) Subretinal drusenoid deposits: further characterization by lipid histochemistry. *Retina* **34,** 825–826
14. Wolter, J. R., and Falls, H. F. (1962) Bilateral confluent drusen. *Arch. Ophthalmol.* **68,** 219–226
15. Zweifel, S. A., Spaide, R. F., Curcio, C. A., Malek, G., and Imamura, Y. (2010) Reticular pseudodrusen are subretinal drusenoid deposits. *Ophthalmology* **117,** 303–312
16. Zweifel, S. A., Imamura, Y., Spaide, T. C., Fujiwara, T., and Spaide, R. F. (2010) Prevalence and significance of subretinal drusenoid deposits (reticular pseudodrusen) in age-related macular degeneration. *Ophthalmology* **117,** 1775–1781
17. Curcio, C. A., Messinger, J. D., Sloan, K. R., McGwin, G., Medeiros, N. E., and Spaide, R. F. (2013) Subretinal drusenoid deposits in non-neovascular age-related macular degeneration: morphology, prevalence, topography, and biogenesis model. *Retina* **33,** 265–276
18. Mrejen, S., Sato, T., Curcio, C. A., and Spaide, R. F. (2014) Assessing the cone photoreceptor mosaic in eyes with pseudodrusen and soft drusen *in vivo* using adaptive optics imaging. *Ophthalmology* **121,** 545–551
19. Querques, G., Massamba, N., Srour, M., Boulanger, E., Georges, A., and Souied, E. H. (2014) Impact of reticular pseudodrusen on macular function. *Retina* **34,** 321–329
20. Huisingh, C., McGwin, G., Jr, Neely, D., Zarubina, A., Clark, M., Zhang, Y., Curcio, C. A., and Owsley, C. (2016) The association between subretinal drusenoid deposits in older adults in normal macular health and incident age-related macular degeneration. *Invest. Ophthalmol. Vis. Sci.* **57,** 739–745
21. Zarubina, A. V., Neely, D. C., Clark, M. E., Huisingh, C. E., Samuels, B. C., Zhang, Y., McGwin, G., Jr., Owsley, C., and Curcio, C. A. (2016) Prevalence of subretinal drusenoid deposits in older persons with and without age-related macular degeneration, by multimodal imaging. *Ophthalmology* **123,** 1090–1100
22. Marsiglia, M., Boddu, S., Bearelly, S., Xu, L., Breaux, B. E., Jr, Freund, K. B., Yannuzzi, L. A., and Smith, R. T. (2013) Association between geographic atrophy progression and reticular pseudodrusen in eyes with dry age-related macular degeneration. *Invest. Ophthalmol. Vis. Sci.* **54,** 7362–7369
23. Xu, L., Blonska, A. M., Pumariega, N. M., Bearelly, S., Sohrab, M. A., Hageman, G. S., and Smith, R. T. (2013) Reticular macular disease is associated with multilobular geographic atrophy in age-related macular degeneration. *Retina* **33,** 1850–1862
24. Steinberg, J. S., Auge, J., Jaffe, G. J., Fleckenstein, M., Holz, F. G., Schmitz-Valckenberg, S., and GAP Study Group (2013) Longitudinal analysis of reticular drusen associated with geographic atrophy in age-related macular degeneration. *Invest. Ophthalmol. Vis. Sci.* **54,** 4054–4060
25. Klein, R., Meuer, S. M., Knudtson, M. D., Iyengar, S. K., and Klein, B. E. (2008) The epidemiology of retinal reticular drusen. *Am. J. Ophthalmol.* **145,** 317–326
26. Pumariega, N. M., Smith, R. T., Sohrab, M. A., Letien, V., and Souied, E. H. (2011) A prospective study of reticular macular disease. *Ophthalmology* **118,** 1619–1625
27. Saadane, A., Mast, N., Charvet, C. D., Omarova, S., Zheng, W., Huang, S. S., Kern, T. S., Peachey, N. S., and Pikuleva, I. A. (2014) Retinal and non-ocular abnormalities in Cyp27a1$^{-/-}$ Cyp64a1$^{-/-}$ mice with dysfunctional metabolism of cholesterol. *Am. J. Pathol.* **184,** 2403–2419
28. Liao, W. L., Heo, G. Y., Dodder, N. G., Pikuleva, I. A., and Turko, I. V. (2010) Optimizing the conditions of a multiple reaction monitoring assay for membrane proteins: quantification of cytochrome P450 11A1 and adrenodoxin reductase in bovine adrenal cortex and retina. *Anal. Chem.* **82,** 5760–5767
29. Mast, N., Reem, R., Bederman, I., Huang, S., DiPatre, P. L., Bjorkhem, I., and Pikuleva, I. A. (2011) Cholestenoic acid is an important elimination product of cholesterol in the retina: comparison of retinal cholesterol metabolism with that in the brain. *Invest. Ophthalmol. Vis. Sci.* **52,** 594–603
30. Wang, M., Heo, G. Y., Omarova, S., Pikuleva, I. A., and Turko, I. V. (2012) Sample prefractionation for mass spectrometry quantification of low-abundance membrane proteins. *Anal. Chem.* **84,** 5186–5191
31. Liao, W. L., Heo, G. Y., Dodder, N. G., Reem, R. E., Mast, N., Huang, S., Dipatre, P. L., Turko, I. V., and Pikuleva, I. A. (2011) Quantification of cholesterol-metabolizing P450s CYP27A1 and CYP46A1 in neural tissues reveals a lack of enzyme-product correlations in human retina but not human brain. *J. Proteome Res.* **10,** 241–248
32. Bretillon, L., Thuret, G., Grégoire, S., Acar, N., Joffre, C., Bron, A. M., Gain, P., and Creuzot-Garcher, C. P. (2008) Lipid and fatty acid profile of the retina, retinal pigment epithelium/choroid, and the lacrimal gland, and associations with adipose tissue fatty acids in human subjects. *Exp. Eye Res.* **87,** 521–528

33. Rudolf, M., Malek, G., Messinger, J. D., Clark, M. E., Wang, L., and Curcio, C. A. (2008) Sub-retinal drusenoid deposits in human retina: organization and composition. *Exp. Eye Res.* **87,** 402–408
34. Castanho, M. A., Coutinho, A., and Prieto, M. J. (1992) Absorption and fluorescence spectra of polyene antibiotics in the presence of cholesterol. *J. Biol. Chem.* **267,** 204–209
35. Rudolf, M., and Curcio, C. A. (2009) Esterified cholesterol is highly localized to Bruch's membrane, as revealed by lipid histochemistry in wholemounts of human choroid. *J. Histochem. Cytochem.* **57,** 731–739
36. Guyton, J. R., and Klemp, K. F. (1988) Ultrastructural discrimination of lipid droplets and vesicles in atherosclerosis: value of osmium-thiocarbohydrazide-osmium and tannic acid-paraphenylenediamine techniques. *J. Histochem. Cytochem.* **36,** 1319–1328
37. Chang, C. C., Huh, H. Y., Cadigan, K. M., and Chang, T. Y. (1993) Molecular cloning and functional expression of human acyl-coenzyme A:cholesterol acyltransferase cDNA in mutant Chinese hamster ovary cells. *J. Biol. Chem.* **268,** 20747–20755
38. Cases, S., Novak, S., Zheng, Y. W., Myers, H. M., Lear, S. R., Sande, E., Welch, C. B., Lusis, A. J., Spencer, T. A., Krause, B. R., Erickson, S. K., and Farese, R. V., Jr. (1998) ACAT-2, a second mammalian acyl-CoA:cholesterol acyltransferase: its cloning, expression, and characterization. *J. Biol. Chem.* **273,** 26755–26764
39. Anderson, R. A., Joyce, C., Davis, M., Reagan, J. W., Clark, M., Shelness, G. S., and Rudel, L. L. (1998) Identification of a form of acyl-CoA:cholesterol acyltransferase specific to liver and intestine in nonhuman primates. *J. Biol. Chem.* **273,** 26747–26754
40. Oelkers, P., Behari, A., Cromley, D., Billheimer, J. T., and Sturley, S. L. (1998) Characterization of two human genes encoding acyl coenzyme A:cholesterol acyltransferase-related enzymes. *J. Biol. Chem.* **273,** 26765–26771
41. Buhman, K. K., Chen, H. C., and Farese, R. V., Jr. (2001) The enzymes of neutral lipid synthesis. *J. Biol. Chem.* **276,** 40369–40372
42. Farese, R. V., Jr. (2006) The nine lives of ACAT inhibitors. *Arterioscler. Thromb. Vasc. Biol.* **26,** 1684–1686
43. Glomset, J. A. (1962) The mechanism of the plasma cholesterol esterification reaction: plasma fatty acid transferase. *Biochim. Biophys. Acta* **65,** 128–135
44. Uelmen, P. J., Oka, K., Sullivan, M., Chang, C. C., Chang, T. Y., and Chan, L. (1995) Tissue-specific expression and cholesterol regulation of acyl-coenzyme A:cholesterol acyltransferase (ACAT) in mice: molecular cloning of mouse ACAT cDNA, chromosomal localization, and regulation of ACAT *in vivo* and *in vitro*. *J. Biol. Chem.* **270,** 26192–26201
45. Li, C. M., Presley, J. B., Zhang, X., Dashti, N., Chung, B. H., Medeiros, N. E., Guidry, C., and Curcio, C. A. (2005) Retina expresses microsomal triglyceride transfer protein: implications for age-related maculopathy. *J. Lipid Res.* **46,** 628–640
46. Li, C. M., Chung, B. H., Presley, J. B., Malek, G., Zhang, X., Dashti, N., Li, L., Chen, J., Bradley, K., Kruth, H. S., and Curcio, C. A. (2005) Lipoprotein-like particles and cholesteryl esters in human Bruch's membrane: initial characterization. *Invest. Ophthalmol. Vis. Sci.* **46,** 2576–2586
47. Tserentsoodol, N., Gordiyenko, N. V., Pascual, I., Lee, J. W., Fliesler, S. J., and Rodriguez, I. R. (2006) Intraretinal lipid transport is dependent on high density lipoprotein-like particles and class B scavenger receptors. *Mol. Vis.* **12,** 1319–1333
48. Chang, T. Y., Chang, C. C., Ohgami, N., and Yamauchi, Y. (2006) Cholesterol sensing, trafficking, and esterification. *Annu. Rev. Cell Dev. Biol.* **22,** 129–157
49. Fliesler, S. J. (2015) Cholesterol homeostasis in the retina: seeing is believing. *J. Lipid Res.* **56,** 1–4
50. Dietschy, J. M., and Turley, S. D. (2002) Control of cholesterol turnover in the mouse. *J. Biol. Chem.* **277,** 3801–3804
51. Björkhem, I., Miettinen, T., Reihnér, E., Ewerth, S., Angelin, B., and Einarsson, K. (1987) Correlation between serum levels of some cholesterol precursors and activity of HMG-CoA reductase in human liver. *J. Lipid Res.* **28,** 1137–1143
52. Björkhem, I., and Hansson, M. (2010) Cerebrotendinous xanthomatosis: an inborn error in bile acid synthesis with defined mutations but still a challenge. *Biochem. Biophys. Res. Commun.* **396,** 46–49
53. Elner, V. M. (2002) Retinal pigment epithelial acid lipase activity and lipoprotein receptors: effects of dietary omega-3 fatty acids. *Trans. Am. Ophthalmol. Soc.* **100,** 301–338
54. Lee, J. W., Fuda, H., Javitt, N. B., Strott, C. A., and Rodriguez, I. R. (2006) Expression and localization of sterol 27-hydroxylase (CYP27A1) in monkey retina. *Exp. Eye Res.* **83,** 465–469
55. Tabas, I. (2002) Consequences of cellular cholesterol accumulation: basic concepts and physiological implications. *J. Clin. Invest.* **110,** 905–911
56. Accad, M., Smith, S. J., Newland, D. L., Sanan, D. A., King, L. E., Jr, Linton, M. F., Fazio, S., and Farese, R. V., Jr. (2000) Massive xanthomatosis and altered composition of atherosclerotic lesions in hyperlipidemic mice lacking acyl CoA:cholesterol acyltransferase 1. *J. Clin. Invest.* **105,** 711–719
57. Yagyu, H., Kitamine, T., Osuga, J., Tozawa, R., Chen, Z., Kaji, Y., Oka, T., Perrey, S., Tamura, Y., Ohashi, K., Okazaki, H., Yahagi, N., Shionoiri, F., Iizuka, Y., Harada, K., *et al.* (2000) Absence of ACAT-1 attenuates atherosclerosis but causes dry eye and cutaneous xanthomatosis in mice with congenital hyperlipidemia. *J. Biol. Chem.* **275,** 21324–21330
58. Fazio, S., Major, A. S., Swift, L. L., Gleaves, L. A., Accad, M., Linton, M. F., and Farese, R. V., Jr. (2001) Increased atherosclerosis in LDL receptor-null mice lacking ACAT1 in macrophages. *J. Clin. Invest.* **107,** 163–171
59. Khelef, N., Buton, X., Beatini, N., Wang, H., Meiner, V., Chang, T. Y., Farese, R. V., Jr, Maxfield, F. R., and Tabas, I. (1998) Immunolocalization of acyl-coenzyme A:cholesterol *O*-acyltransferase in macrophages. *J. Biol. Chem.* **273,** 11218–11224
60. Sakashita, N., Miyazaki, A., Takeya, M., Horiuchi, S., Chang, C. C., Chang, T. Y., and Takahashi, K. (2000) Localization of human acyl-coenzyme A:cholesterol acyltransferase-(ACAT-1) in macrophages and in various tissues. *Am. J. Pathol.* **156,** 227–236
61. Sakashita, N., Chang, C. C., Lei, X., Fujiwara, Y., Takeya, M., and Chang, T. Y. (2010) Cholesterol loading in macrophages stimulates formation of ER-derived vesicles with elevated ACAT1 activity. *J. Lipid Res.* **51,** 1263–1272
62. Li, L., and Pownall, H. J. (2000) Regulation of acyl-coenzyme A:cholesterol acyltransferase (ACAT) synthesis, degradation, and translocation by high-density lipoprotein(2) at a low concentration. *Arterioscler. Thromb. Vasc. Biol.* **20,** 2636–2642
63. Lei, X., Fujiwara, Y., Chang, C. C., Chang, T. Y., Takeya, M., and Sakashita, N. (2010) Association of ACAT1-positive vesicles with late endosomes/lysosomes in cholesterol-rich human macrophages. *J. Atheroscler. Thromb.* **17,** 740–750
64. Amaratunga, A., Abraham, C. R., Edwards, R. B., Sandell, J. H., Schreiber, B. M., and Fine, R. E. (1996) Apolipoprotein E is synthesized in the retina by Muller glial cells, secreted into the vitreous, and rapidly transported into the optic nerve by retinal ganglion cells. *J. Biol. Chem.* **271,** 5628–5632
65. Kuhrt, H., Härtig, W., Grimm, D., Faude, F., Kasper, M., and Reichenbach, A. (1997) Changes in CD44 and ApoE immunoreactivities due to retinal pathology of man and rat. *J. Hirnforsch.* **38,** 223–229
66. Shanmugaratnam, J., Berg, E., Kimerer, L., Johnson, R. J., Amaratunga, A., Schreiber, B. M., and Fine, R. E. (1997) Retinal Muller glia secrete apolipoproteins E and J, which are efficiently assembled into lipoprotein particles. *Brain Res. Mol. Brain Res.* **50,** 113–120
67. Anderson, D. H., Ozaki, S., Nealon, M., Neitz, J., Mullins, R. F., Hageman, G. S., and Johnson, L. V. (2001) Local cellular sources of apolipoprotein E in the human retina and retinal pigmented epithelium: implications for the process of drusen formation. *Am. J. Ophthal.* **131,** 767–781
68. Hirsch-Reinshagen, V., Donkin, J., Stukas, S., Chan, J., Wilkinson, A., Fan, J., Parks, J. S., Kuivenhoven, J. A., Lütjohann, D., Pritchard, H., and Wellington, C. L. (2009) LCAT synthesized by primary astrocytes esterifies cholesterol on glia-derived lipoproteins. *J. Lipid Res.* **50,** 885–893
69. Pfrieger, F. W., and Ungerer, N. (2011) Cholesterol metabolism in neurons and astrocytes. *Prog. Lipid Res.* **50,** 357–371
70. Saade, C., and Smith, R. T. (2014) Reticular macular lesions: a review of the phenotypic hallmarks and their clinical significance. *Clin. Experiment. Ophthalmol.* **42,** 865–874
71. Meiner, V. L., Cases, S., Myers, H. M., Sande, E. R., Bellosta, S., Schambelan, M., Pitas, R. E., McGuire, J., Herz, J., and Farese, R. V., Jr. (1996) Disruption of the acyl-CoA:cholesterol acyltransferase gene in mice: evi-

dence suggesting multiple cholesterol esterification enzymes in mammals. *Proc. Natl. Acad. Sci. U.S.A.* **93,** 14041–14046

72. Omarova, S., Charvet, C. D., Reem, R. E., Mast, N., Zheng, W., Huang, S., Peachey, N. S., and Pikuleva, I. A. (2012) Abnormal vascularization in mouse retina with dysregulated retinal cholesterol homeostasis. *J. Clin. Invest.* **122,** 3012–3023
73. Charvet, C. D., Saadane, A., Wang, M., Salomon, R. G., Brunengraber, H., Turko, I. V., and Pikuleva, I. A. (2013) Pretreatment with pyridoxamine mitigates isolevuglandin-associated retinal effects in mice exposed to bright light. *J. Biol. Chem.* **288,** 29267–29280
74. Maeda, A., Maeda, T., Sun, W., Zhang, H., Baehr, W., and Palczewski, K. (2007) Redundant and unique roles of retinol dehydrogenases in the mouse retina. *Proc. Natl. Acad. Sci. U.S.A.* **104,** 19565–19570
75. Cui, W., Taub, D. D., and Gardner, K. (2007) qPrimerDepot: a primer database for quantitative real time PCR. *Nucleic Acids Res.* **35,** D805–D809